

Valentin R. Troll · Peter M. Sachs
Hans-Ulrich Schmincke · Mari Sumita

The REE-Ti mineral chevkinite in comenditic magmas from Gran Canaria, Spain: a SYXRF-probe study

Received: 17 July 2001 / Accepted: 3 April 2003 / Published online: 12 August 2003
© Springer-Verlag 2003

Abstract The REE-Ti silicate chevkinite has been recognised previously in Miocene ignimbrites from Gran Canaria, and in correlative offshore syn-ignimbrite turbidites. We have estimated the partition coefficients of REE, Y, Zr and Nb for chevkinite and co-existing peralkaline rhyolitic (comendite) glass using synchrotron-XRF-probe analyses (SYXRF) in order to evaluate the role of this mineral in the REE budget of felsic peralkaline magmas. The Zr/Nb ratio of the chevkinite is 1.55–1.7, strongly contrasting with Zr/Nb of 6.5 in the associated glass. Zr shows a three-fold enrichment in chevkinite relative to the residual melt, whereas Nb is enriched by a factor > 10 . The enrichment of Ce and La in chevkinite is even more significant, namely 19 wt(%) Ce and 12 wt(%) La, compared to 236 ppm Ce and 119 ppm La in the glass. Chevkinite/glass ratios are 988 ± 30 for La, 806 ± 30 for Ce, 626 ± 30 for Pr, 615 ± 40 for Nd, 392 ± 50 for Sm, 225 ± 30 for Eu, 142 ± 25 for Gd, 72 ± 20 for Dy. For trace elements, we derived $K_{d_{TE}}$ of 74 ± 25 for Y, > 8 for Hf, > 50 for Th, 15 ± 5 for Nb and 3.55 ± 0.4 for Zr. Mineral/glass ratios for co-existing titanite are 28 ± 10 for La, 86 ± 20 for Ce, 98 ± 30 for Pr, 134 ± 35 for Nd, 240 ± 50 for Sm, 50 ± 20 for Eu, 96 ± 25 for Gd, 82 ± 25 for Dy, 99 ± 30 for Y, 45 ± 10 for Nb and 3 ± 0.5 for Zr. Based on these data, the removal of only 0.05 wt% of chevkinite from a magma with initially 300 ppm Ce would deplete the melt by 93 ppm to yield 207 ppm Ce in the residual liquid. Chevkinite thus appears, when present, to be the con-

trolling mineral within the LREE budget of evolved peralkaline magmas.

Introduction

Chevkinite and the closely related perrierite have been widely recognised in plutonic and volcanic rocks worldwide (e.g. Virginia/USA, Mitchell 1966; Colorado/USA, Izett and Wilcox 1968; Gran Canaria/Spain, Schmincke 1976; New South Wales/Australia, Ewart 1981; La Primavera/Mexico, Mahood 1981; St Kilda/Scotland, Harding et al. 1982; Paraguay/South America, Haggerty and Mariano 1983; Nigeria/Africa, Bennett et al. 1984; Mt Amiata/Italy, van Bergen 1984; Shikoku Island/Japan, Imaoka and Nakashima 1994; Nevada/USA, Robinson and Miller 1999; Kenya/Africa, Scaillett and Macdonald 2001; Macdonald et al. 2002). Chevkinite and perrierite [$A_4 B_1 C_2 D_2 Si_4 O_{22}$ where A = REE, Ca, Sr, Na, K, Th; B = Fe^{2+} , Mg, Mn, Ca; C = Ti, Mg, Mn, Fe, Nb, Zr and D = Ti] are both C2/m and can be safely distinguished only by their β -angle (Haggerty and Mariano 1983), but chemical discrimination using the average ionic radius of the A, B and C lattice site (Ito 1967; Segalstad and Larsen 1978) are also widely used. It has been questioned whether perrierite is a valid species (e.g. Jaffe et al. 1956) but Mitchell (1966) and Ito (1967) showed that perrierite and chevkinite are separate but closely related species. Mitchell (1966) also noted that chevkinite forms from perrierite below 600 °C. Both minerals occur, however, side by side in the Björkedalen pegmatite in Norway (Segalstad and Larsen 1978), suggesting that controls other than temperature may also be relevant. Ignimbrites erupted at high temperature are, according to Mitchell (1966), likely to contain perrierite as the stable REE-phase but both phases were reported in fallout ash-beds from several locations (e.g. Izett and Wilcox 1968; Ewart 1981). The mineral phase we studied can be classified as chevkinite, using the chemical discrimination suggested by Ito (1967) for

Editorial responsibility: I. Parsons

V. R. Troll (✉) · P. M. Sachs
H.-U. Schmincke · M. Sumita
Abt. Vulkanologie und Petrologie, GEOMAR Forschungszentrum, Wischhofstraße 1–3, 24148 Kiel, Germany
E-mail: trollv@tcd.ie
Tel.: +353-1-6083856
Fax: +353-1-6081199

Present address: V. R. Troll
Dept. of Geology, University of Dublin, Trinity College,
Dublin 2, Ireland

synthetic chevkinites and perrierites and that of Segalstad and Larsen (1978) for natural ones (both methods are based on the average ionic radius of the elements that occupy the A, B, and C sites of the crystal lattice). However, in the approach of Segalstad and Larsen (1978) the phase under study is close to the chevkinite-perrierite transition. In the absence of diagnostic XRD evidence, we refer to the crystals studied as chevkinite.

Chevkinite is characterised by a strong preference for REE in the crystal structure and is thought to greatly influence the REE budget of evolved magmas by reducing the relative concentration of otherwise incompatible REE (e.g. La, Ce, Nd) and Nb, Zr and Y in residual melts. Chevkinite and perrierite minerals, besides a range of other accessory phases, can also host U and Th and are important for isotope systematics as well as trace element modelling and melt evolution. On the other hand, chevkinite and perrierite may act as a refractory phase during partial melting and assimilation of wall-rocks and hold back the elements compatible in the mineral (Green and Pearson 1988). Due to the lack of natural partition coefficients (K_d) for chevkinite and co-existing accessory minerals and their equilibrium melt, the role of chevkinite can only be evaluated qualitatively using experimentally-derived partition coefficients for extremely REE-enriched melt compositions and their precipitates (Green and Pearson 1988). In order to quantify the possibly major impact of chevkinite on the REE and trace element budget of evolved alkaline magmas, detailed partition coefficients (K_d) for these elements are required, so that models may be more truly representative of petrogenetic processes (cf. Brooks et al. 1981; Wolff and Storey 1984). To measure partition coefficients between natural chevkinite and its melt, we studied chevkinite and co-existing comenditic rhyolite glass and groundmass from onshore ignimbrite samples and syn-ignimbrite turbidites (ODP Leg 157, Sumita and Schmincke 1998), using synchrotron-XRF-microprobe analysis (SYXRF) at HASYLAB, DESY in Hamburg. Since chevkinite is often accompanied by other REE-bearing phases, which may affect the REE budgets, we also analysed co-existing titanite.

Analytical methods

Samples were prepared as polished thin and doubly-polished thick sections for optical microscopy, electron microprobe analysis, and SYXRF microprobe analysis.

XRF and ICPMS: Whole rocks and fiamme matrix glass of the host ignimbrites were analysed for major and trace elements by XRF at GEOMAR, using an automated Phillips PW1480 spectrometer. All analyses were performed with a Rh tube; calibration was performed using international geological reference samples. Trace elements and REE were analysed by ICP-MS on a Perkin Elmer Sciex ELAN 5000 at Actlabs Ancaster, Ontario/ Canada (Errors for REE are given with ± 5 ppm, compare: <http://www.actlabs.com>).

Electron microprobe (EMP): Mineral analyses were performed on a Cameca SX-50 electron microprobe at GEOMAR, applying

the built-in PAP correction procedure (Pouchou and Pichoir 1984). Analytical conditions included an acceleration voltage of 15 kV, a beam current of 8–20 nA, and counting times of between 20–60 s on peaks. A focused beam of 1–5 μm^2 was used for minerals, and a rastered beam of 5–40 μm^2 for glass to minimise Na loss. Na migration under the probe beam was assessed by monitoring the stability of Na counts during the analysis. Relative analytical precision [(standard deviation/mean) $\times 100$] was better than 3% for Si, Al, Ca, Na and K, better than 4% for Ti and Fe, and better than 10% for Mg, based on repeated analysis of natural and synthetic mineral and glass standards (wollastonite, andradite, rutile and various synthetic REE-glasses).

Synchrotron microprobe (SYXRF-probe): Trace and rare earth element compositions in chevkinite, titanite and glass were analysed with synchrotron-XRF microprobe (SYXRF) at the DORIS positron storage facility at HASYLAB/DESY in Hamburg (Troll et al. 1999). Experimental setup and quantification of the spectra are described in Lechtenberg et al. (1996).

Cleaned crystals and glass shards were mounted onto the tip of a glass fibre so that they were “free hanging” to prevent the beam from passing through any surrounding or underlying matrix. The primary synchrotron beam was collimated to either 50 \times 50 μm^2 or 30 \times 30 μm^2 and passed through a 100- μm -thick Cu foil. All measurements were performed in air; spectra were recorded with a HP Ge detector. Counting times were 1,000–3,600 s. Data reduction was performed using the fundamental parameter method (Janssens et al. 1993; Vincze et al. 1993). Quantification of spectra was performed using EMP-determined Fe concentrations as scaling parameter because Fe proved to be fairly constant throughout the chevkinite sample suite (Fe wt% in chevkinite of ignimbrite “A” = 7.59 \pm 0.22, n = 22 and Fe wt% in chevkinite from ignimbrite “X” = 7.29 \pm 0.19, n = 36). Precision and accuracy of the analyses were tested using international standards previously analysed by Hansteen et al. (2000). Detection limits are for atomic numbers 21(Sc)–26 (Co): 0.1–3 $\mu\text{g/g}$; 28(Ni)–60 (Nd): 0.1–1 $\mu\text{g/g}$; > 60(Nd): ca. 5 $\mu\text{g/g}$. Analytical accuracy was checked by analysis of international standards (analytical signal $K\alpha$ for all elements except Th and Pb: $L\alpha$; Hansteen et al. 2000; Sachs and Hansteen 2000), and is better than 5% at concentrations < 100 $\mu\text{g/g}$, and better than 15% at < 10 $\mu\text{g/g}$.

Geological setting

Gran Canaria, ca. 200 km off the NW African coast, is one of the central islands of the Canary ocean island chain. The archipelago is thought to originate from a long-lived melting anomaly beneath the passive margin of the African continent (e.g. Schmincke 1976; Hoernle and Schmincke 1993).

The Miocene basaltic shield of Gran Canaria (ca. 14–15 Ma) is overlain by about 20 peralkaline trachytic to rhyolitic (comenditic to pantelleritic) ignimbrites (Mogan Group, ca. 13.95–13.35 Ma; Bogaard and Schmincke 1998). The base of the Mogan Group is marked by the strongly zoned rhyolite-trachyte-basalt ignimbrite “P1”, interpreted to have experienced fractional crystallisation and magma mixing as well as contamination by interaction with felsic plutonics of the island’s core (Freundt and Schmincke 1995). Further details of the stratigraphy, mineralogy and overall geochemistry of the Miocene ignimbrite succession can be found in Schmincke (1969, 1976, 1997); Crisp and Spera (1987); Cousens et al. (1990); Freundt and Schmincke (1995); Sumita and Schmincke (1998); and Troll and Schmincke (2002).

Petrology

Mineralogy of host ignimbrites

The ignimbrite cooling units of the Mogan Group are, without exception, compositionally zoned, with a more mafic composition at the top, and consist of two or more chemical and mineralogical end-members (Schmincke 1997). This vertical zonation is thought to reflect successive tapping of vertically stratified magma reservoirs, with the more mafic magma end-member(s) being at lower stratigraphic levels within such a reservoir and consequently erupted late during evacuation of the magma chamber (cf. Blake 1981).

Chevkinite occurs in several of the Miocene peralkaline ignimbrites on Gran Canaria (ignimbrites "P1", "P2", "X", "A"). We have examined two prominent ignimbrites of the Middle and Upper Mogan formations—ignimbrite "X" (13.71 ± 0.03 Ma) and ignimbrite "A" (13.63 ± 0.03 Ma); Bogaard and Schmincke (1998)—selected because their stratigraphy, depositional history and geochemistry have been studied in detail previously.

Ignimbrite "X" shows an extremely crystal-enriched fallout tuff at the base, followed by several flow units of comenditic rhyolite (Sumita et al. in prep.). Some flow units are enriched in syenite xenoliths and/or trachyte fiamme. The rhyolite end-member of ignimbrite "X" is crystal-rich (>40 vol%) and shows a phenocryst assemblage of anorthoclase, aegirine-augite, alkali-amphibole, titanite, chevkinite and Fe-Ti oxides, whereas the trachyte is characterised by mainly oligoclase, augite and amphibole, characteristically lacking chevkinite phenocrysts.

Ignimbrite "A" contains up to 25 vol% of anorthoclase, alkali-amphibole, phlogopite, aegirine-augite, Fe-Ti oxide and accessory chevkinite in most evolved rhyolite pumice(s) and oligoclase, amphibole and subordinate phlogopite in the trachyte end-member. Chevkinite in ignimbrite "A" occurs as inclusions in amphibole and associated with Fe-Ti oxide clusters. It is not found as inclusions in feldspar in either of the two ignimbrites, although feldspar commonly displays a longer crystallisation interval than, for example, the amphibole phenocrysts.

Fresh volcanic glass, representative of the melt composition, is difficult to obtain from these ignimbrites, since the basal vitrophyres are commonly hydrated and former groundmass glass of fiamme has generally suffered high-T devitrification and post-depositional degassing. Fresh rhyolitic glass from ignimbrite "X" was not recovered from onshore samples, but was found together with chevkinite and titanite in syn-ignimbrite turbidites drilled during ODP Leg 157 (Sumita and Schmincke 1998). The glass is believed to have been chilled on contact of the hot pyroclastic flows with seawater followed by rapid burial. In ignimbrite "A", fresh glass is locally found in the basal vitrophyre and chemically resembles groundmass separates from end-member

fiamme. Since ignimbrite "A" is comparatively thin, on the order of 10 m or less in thickness, high-T devitrification is considered less influential on the groundmass bulk composition, which is therefore taken as a reasonable equivalent to the former melt composition.

Chevkinite in ignimbrites "X" and "A"

Ignimbrite "X" contains abundant (perhaps 0.05%), well-developed, needle-like, euhedral prisms of chevkinite up to 600 μm in length plus broken but unresorbed crystal fragments (Fig. 1a), suggesting that they grew "free floating" in the melt and are in chemical equilibrium with the host magma. Chevkinite is less abundant in ignimbrite "A" ($<0.05\%$), and generally occurs as small inclusions (up to 50 μm) in edenitic amphibole in the rhyolite end-member magmas or as rounded crystals associated with Fe-Ti-oxide clusters (Fig. 1b, c).

Chevkinite crystals in ignimbrites "X" and "A" are optically unzoned (homogeneous) and are strongly pleochroic, ranging from intense brown to deep black. The pleochroism shows the chevkinite crystals to be non-metamict. The crystals show high relief and high birefringence (>0.07).

Crystallisation conditions (intensive parameters)

Temperature

Applying the temperature-sensitive exchange reaction of Na and K between amphibole and melt of Helz (1979) to the compositions of Gran Canaria ignimbrites, we derived maximum temperatures of 780 ± 25 °C for ignimbrite "X" comenditic rhyolite and 765 ± 25 °C for ignimbrite "A" comenditic rhyolites. These results agree with minimum homogenization temperatures of melt inclusions obtained from ignimbrite "A" (Troll and Schmincke 2002) that cluster around 760 ± 40 °C for rhyolitic melt inclusions in anorthoclase feldspar (calculated after Thomas, 1990). For the trachyte end-member of ignimbrite "A" we derived an approximate temperature of 830 ± 30 °C using the methods of Helz (1979) and Thomas (1990).

Pressure

Pressure estimates were obtained employing the "Al-in-amphibole" barometer (Johnson and Rutherford 1989; Anderson and Smith 1995). Our results indicate a total pressure of ca. 1.75 ± 0.5 kb for ignimbrite "A" and 2.1 ± 0.6 kb¹ for ignimbrite "X". The pressure estimates are consistent with previous estimates on ignimbrite "A" (Crisp and Spera 1984) and with the results of Freundt and Schmincke (1995) who derived crystallisation

¹Calculated from mineral data of Sumita and Schmincke (1998).

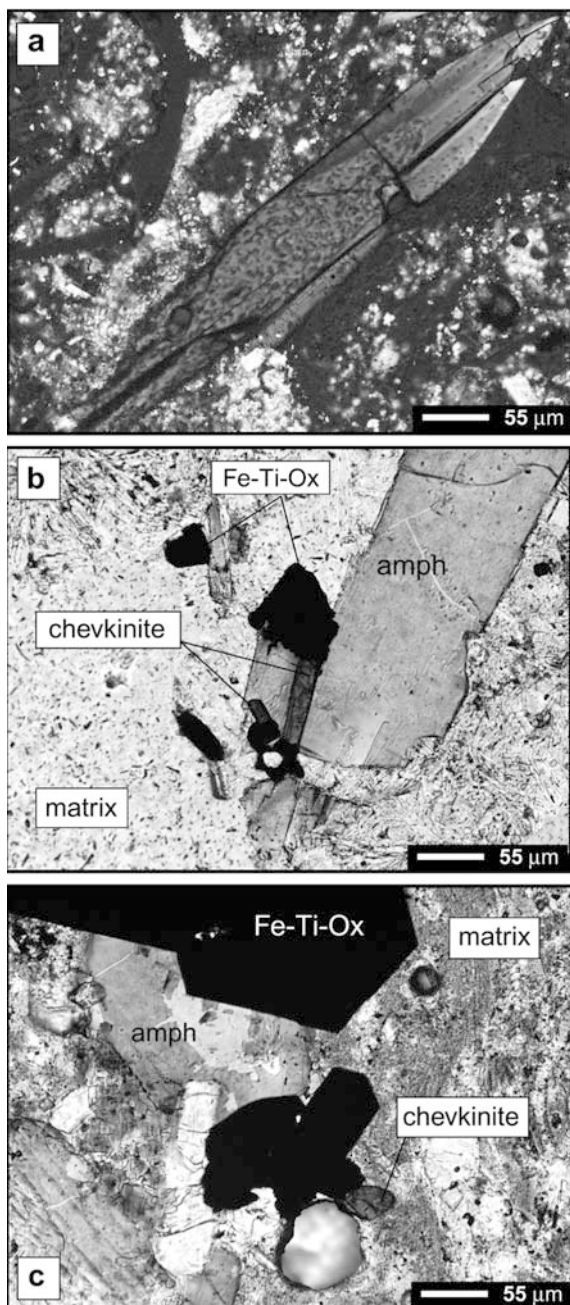


Fig. 1 **a** Photomicrograph (crossed polarisers) of euhedral chevkinite crystal in syn-ignimbrite “X” turbidite (sample 67R-4 53–59 drilled during ODP Leg 157, site 953; Sumita and Schmincke 1998). Partition coefficients were determined from an average of three analysis of this crystal and an average of three associated glass shard analyses. **b** Photomicrograph of chevkinite inclusion in amphibole of ignimbrite “A” (plane polarised light). **c** Photomicrograph of rounded chevkinite grain associated with Fe-Ti Oxide clusters of ignimbrite “A” (plane polarised light)

pressures of 1–2 kb for the rhyolites of the lower Mogan composite ignimbrite “P1”.

Oxygen fugacity

Oxygen fugacities for the rhyolite and trachyte compositions were estimated following the formulation of Wones

(1982, 1989) that is based on thermodynamic data for the system titanite-magnetite-quartz, since only magnetite is present in “A”, preventing application of ilmenite-magnetite equilibria. The results define a curve of FMQ + 1 for the trachyte that slightly increases in oxidation towards the rhyolite compositions (FMQ + 1.2), with approximate values of $\log f_{\text{O}_2} = -12$ at 830 °C and $\log f_{\text{O}_2} = -14$ at 775 °C, respectively. This agrees well with the oxygen fugacities of $\log f_{\text{O}_2} = -11$ to -13 for trachytes and rhyolites of “P1” ignimbrite at 850 °C, which range from approximately FMQ + 1 to +1.5, respectively (Freundt and Schmincke, 1995) and are based on Fe-Ti oxide mineralogy.

H₂O content

Recent studies on several ignimbrites have shown that H₂O contents in the Mogan rhyolites may well exceed 4 wt%, as reported for “P1” (Freundt and Schmincke 1995). In ignimbrite “A” samples, H₂O concentrations range from 1.5–3% in trachyte and from 3–4% in rhyolite, based on melt inclusions in alkali-feldspar (Troll and Schmincke 2002). With approximately 2–4 wt% H₂O, the Mogan rhyolites were still water-undersaturated at the given crystallisation pressures and temperatures judging from the experimental water solubility curve of e.g. Silver et al. (1990). The H₂O concentrations of Mogan ignimbrites were thus somewhat higher than the 1–2.5 wt% H₂O previously suggested by Crisp and Spera (1984).

Geochemistry of host ignimbrites

Ignimbrites “X” and “A” are both comenditic and comprise various trachyte and rhyolite end-member compositions. Major element systematics commonly show a decrease in MgO, TiO₂, Al₂O₃, CaO and P₂O₅ with increasing degree of differentiation, suggesting a straightforward fractional crystallisation sequence by dominantly oligoclase to anorthoclase feldspar removal and smaller proportions of ferromagnesian phases (clinopyroxene, amphibole, Fe-Ti-oxides) (Fig. 2a).

Ignimbrite “X” comprises a trachyte and a rhyolite end-member composition which both plot in the comendite fields of Macdonald (1974). Ce and La concentrations of trachyte groundmass yield values of 203 and 184 ppm respectively, whereas the rhyolite glass measured by SYXRF (cf. Table 1) shows 230–300 and 119–160 ppm Ce and La, respectively. This implies an enrichment of Ce during differentiation from trachyte to rhyolite on the order of 30–100 ppm. The same differentiation process slightly depleted La in the melt by about 25–65 ppm.

Ignimbrite “A”, in turn, consists of three end-members: a comenditic trachyte (CT), a comenditic rhyolite (CR) and an evolved comenditic rhyolite (RF2). The groundmass of trachyte CT contains on average 175 ppm Ce and about 90 ppm La. Rhyolite CR groundmass

Fig. 2 a Major element classification diagram of Macdonald (1974) for ignimbrite "A" whole rocks and fiamme. The samples follow a single evolutionary sequence from comenditic trachyte CT (squares) through comenditic rhyolite CR (circles) to evolved comenditic rhyolite RF2 (light-coloured triangles). Ignimbrite "X" major element data (grey field) virtually occupy the same compositional fields in Al_2O_3 - FeO_t space. **b** Pb/Ce vs Ce (ppm) of ignimbrite "A" magmatic end-members (whole rocks and groundmass). Ce concentrations increase from trachyte CT to rhyolite CR coupled with increasing Pb/Ce ratios, whereas Ce concentrations decrease from rhyolite CR to rhyolite RF2, although Pb/Ce still increases. **c** Chondrite normalised spider plot of REE of ignimbrite "A" magmatic end-members. While trachyte CT to rhyolite CR shows a relative enrichment of all REE, rhyolite RF2 shows a depletion of these elements relative to rhyolite CR, with concentrations similar to the CT trachyte end-member

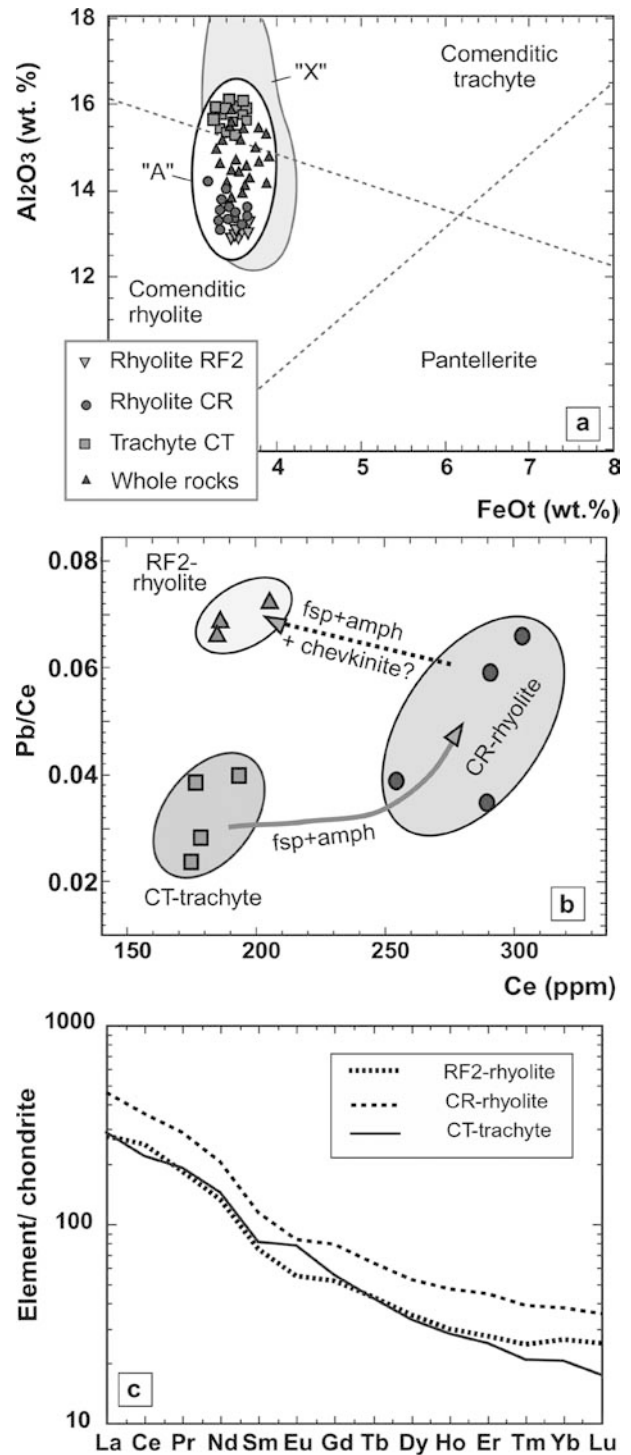
separates yield Ce 290–300 ppm and La 125 ppm, whereas rhyolite RF2 groundmass contains Ce ~150 ppm and La 65–70 ppm. The differentiation processes that acted in ignimbrite "A" magmas thus reduced Ce and La from trachyte to the final differentiation product rhyolite RF2. Rhyolite CR, however, shows a strong enrichment of these elements. This suggests crystallisation of chevkinite during the fractionation interval from rhyolite CR to rhyolite RF2, but not in trachyte CT.

The effects of potential chevkinite fractionation are particularly well reflected by an increase in element ratios such as Pb/Ce (vs. Ce), Pb/La (vs. La) and, Zr/Nb (vs. Nb) from trachyte CT to its rhyolite CR respectively. Rhyolite RF2, in turn, yields higher Pb/Ce, Pb/La and Zr/Nb, although the actual concentrations of Ce, La and Zr in the rock are lower than observed in the CR end-member. We infer that these changes in element concentrations and ratios in the ignimbrite "A" end-members (Fig. 2b, c) have resulted from chevkinite fractionation from the melt and some assimilation of a wall rock partial melt (see below).

Sample selection

Chevkinite crystallisation in ignimbrite "A" occurred over a comparatively short fractionation interval (mainly restricted to RF2-rhyolite), whereas in ignimbrite "X" chevkinite crystallisation is evident in all rhyolite samples. Moreover, "A" shows evidence for contamination of the rhyolite end-member magmas during a late stage of evolution. $\delta^{18}O$ of feldspar separates from rhyolite fiamme of ignimbrite "A" range from 6.3–7.3 (± 0.1)‰ over an SiO_2 range of only 5 wt% (Troll and Schmincke 2002). This change clearly exceeds the rate of closed system fractionation predicted by Hoefs (1996) being on the order of 0.2–0.4‰ over a range of 5 wt% SiO_2 . Moreover, oxygen isotope ratios for ignimbrite "A" feldspar separates correlate positively with Sr isotope ratios, consistent with late stage contamination (Troll 2001).

Feldspar separates from a trachyte and rhyolite fiamme and the basal rhyolitic fallout tuff of ignimbrite "X", analysed by C. Harris at the University of Cape-



town (see Harris et al. 2000 for analytical details), show $\delta^{18}O$ values (VSMOW) of 6.24 (± 0.1)‰ for the trachyte-derived feldspars and 6.29 and 6.34 (± 0.1)‰ for feldspar separates from rhyolite compositions. This is well within the range of $\delta^{18}O$ values expected for a rock suite that fractionated under fairly closed-system conditions over a narrow SiO_2 range. For these reasons, ignimbrite "A" chevkinite has not been considered for Kd calculations, since element concentrations in the melt may have been modified by input of a partial melt of wall rock during

Table 1 Representative analysis of minerals, groundmass and glass

Oxide (wt%)	Chevkinite "X" EMP	Titanite "X" EMP	Chevkinite "A" EMP	Oxide (wt%)	"X" Rhyolite glass EMP	"X"-TF1-GM ^a XRF	"A"-F1-GM ^a XRF	"A"-F31-GM ^a XRF
SiO ₂	19.96	29.03	20.09	SiO ₂	68.55	65.38	70.91	70.01
TiO ₂	18.42	34.33	18.47	TiO ₂	0.76	0.98	0.54	0.56
Al ₂ O ₃	0.16	0.23	0.29	Al ₂ O ₃	13.61	14.16	13.27	13.56
FeOt	9.37	3.31	9.77	FeOt	3.28	4.65	3.55	3.37
MnO	0.32	0.55	0.24	MnO	0.3	0.22	0.16	0.16
MgO	0.62	n.d.	0.42	MgO	0.54	0.83	0.16	0.21
CaO	3.32	24.13	3.60	CaO	0.36	0.95	0.24	0.28
Na ₂ O	n.d.	0.60	n.d.	Na ₂ O	5.28	6.46	6.15	6.18
K ₂ O	n.d.	0.02	n.d.	K ₂ O	3.75	4.77	4.88	4.66
F	n.d.	0.44	n.d.	P ₂ O ₅	0.09	0.08	0.03	0.04
				Total	96.52	98.5	99.89	99.03
Oxide (wt%)	SYXRF ^b	SYXRF ^b	SYXRF ^c	(ppm)	SYXRF ^b	ICPMS	ICPMS	ICPMS
La ₂ O ₃	13.79	0.40	13.89	La	119.2	184	73	125
Ce ₂ O ₃	22.26	2.39	22.28	Ce	235.8	203	149	260
Pr ₂ O ₃	1.98	0.31	2.03	Pr	27.1	39.7	16.3	25.4
Nd ₂ O ₃	7.46	1.63	7.33	Nd	103.7	145	65.2	94.6
Sm ₂ O ₃	0.77	0.47	0.59	Sm	17	24	11.7	15.2
Eu ₂ O ₃	0.13	0.03	0.08	Eu	5	6.03	2.99	3.78
Gd ₂ O ₃	0.39	0.27	0.22	Gd	23.7	20.4	10.6	12.8
Dy ₂ O ₃	0.17	0.20	0.07	Dy	20.6	18.4	8.6	8.8
Er ₂ O ₃	n.d. ^d	0.07	0.02	Er	< 5	9.77	4.34	4.44
Y ₂ O ₃	0.71	0.95	0.25	Sr	6	13	8	5
ZrO ₂	0.55	0.49	0.35	Y	75.4	117	2.5	42.7
Nb ₂ O ₅	0.38	1.04	0.22	Zr	1,161	840	673	1,040
HfO ₂	0.01	n.d.	0.02	Nb	178	185	52	123
ThO ₂	0.08	n.d.	0.05	Hf	< 10	20	18.9	24.9
Total	100.85	100.89	100.27	Th	< 15	11.8	16.9	21.5

^aGroundmass^bAverage of three analyses^cAverage of two analyses

n.d., Not detected

and following chevkinite crystallisation. Ignimbrite "X", on the other hand, is thought to more truly reflect "closed system" element partitioning between chevkinite and an equilibrium rhyolite melt. The analyses chosen for Kd calculation were taken from a particularly well-developed euhedral crystal (Fig. 1a) and an average of three glass-shard analyses taken from the same sample. The crystal was chemically unzoned and shows virtually the same major element composition as eight other chevkinite crystals from the same ignimbrite studied by EMP. The glass was fresh at high magnification under the stereomicroscope and the optical microscope and yielded major element concentrations very similar to those published by Sumita and Schmincke (1998) on the same unit.

Mineral chemistry and trace element ratios in chevkinite and glass

Minerals and glass were first analysed by EMP for major oxide concentrations and subsequently by SYXRF for rare earth and trace elements. Groundmass separates were analysed by XRF for major elements and by ICP-MS for trace and RE elements. A total of 58 chevkinite analyses was carried out with EMP and 11 chevkinite

analyses were performed with SYXRF. Representative results of combined EMP, XRF, SYXRF and ICP-MS analyses for chevkinite, titanite and glass/groundmass from "X" and chevkinite and groundmass from ignimbrite "A" are given in Table 1. A synchrotron spectrum of chevkinite from ignimbrite "X", recorded during data acquisition and subsequently used for element quantification, is given in Fig. 3.

Structural formulae for the chevkinites are given in Table 2. In both cases, the formulae conform closely to the theoretical $A_4 B_1 C_2 D_2 Si_4 O_{22}$. Cation sums are 13.2 and the total positive charges are within 0.01 of the theoretical 44, strongly suggesting that our analyses are of good quality and that the chevkinites are close to stoichiometric.

The slight excess of cations in the A site (0.3) and deficiency in the C site (0.2) are found in many chevkinites and perrierites and may indicate that some Ca can enter the B site, causing displacement of Fe to the C site (R. Macdonald, personal communication 2001).

Chevkinite and glass in ignimbrites "X" and "A"

The Zr/Nb ratio of the chevkinite in "X" is 1.55, strongly contrasting with 6.5 in the glass. Zr shows a

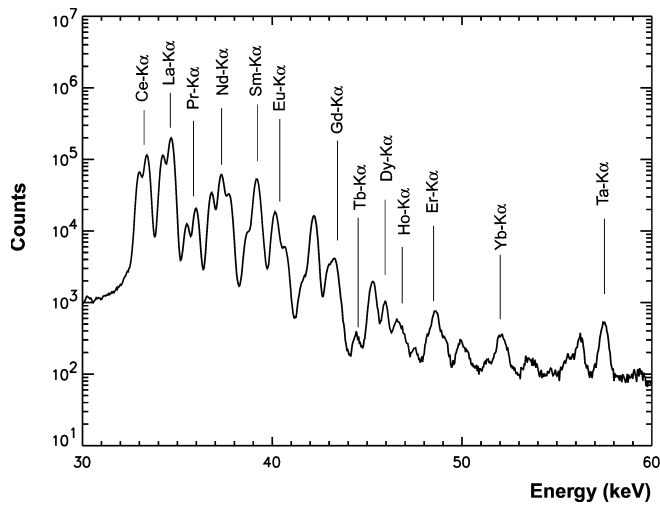


Fig. 3 Synchrotron spectrum showing REE peaks of chevkinite from ignimbrite "X" (see also Fig. 1a). K_{α} REE peaks used for quantification are indicated

Table 2 Structural formulae, based on 22 oxygens

Crystal	Chevkinite "X"	Chevkinite "A"
La	1.038	1.047
Ce	1.664	1.668
Pr	0.147	0.152
Nd	0.545	0.536
Sm	0.054	0.042
Eu	0.01	0.005
Gd	0.027	0.015
Dy	0.012	0.005
Er	0.00	0.001
Y	0.076	0.027
Ca	0.726	0.789
Th	0.003	0.003
Sum (A-site)	4.302	4.290
Fe ²⁺ (B-site)	1.00	1.00
Fe ²⁺	0.6	0.671
Mn	0.055	0.042
Mg	0.189	0.128
Al	0.039	0.069
Zr	0.055	0.035
Hf	0.001	0.001
Nb	0.038	0.022
Ti	0.828	0.841
Sum (C-site)	1.805	1.809
Ti (D-site)	2	2
Si	4.076	4.107
Σ cations	13.183	13.206

three-fold enrichment in chevkinite relative to the glass, whereas Nb is enriched by a factor >10. The enrichment of Ce and La in chevkinite is even more drastic, ca.19 wt(%) Ce and 12 wt(%) La to about 235 ppm Ce and 120 ppm La in the glass. This implies a significantly lower $K_{d_{chev}}$ for Zr than for Nb, as well as a lower chevkinite/glass ratio for Ce than for La, respectively.

Chevkinite in ignimbrite "A" has a Zr/Nb ratio of ca. 1.7, very similar to chevkinite in ignimbrite "X", however, with significantly lower concentration of Zr and

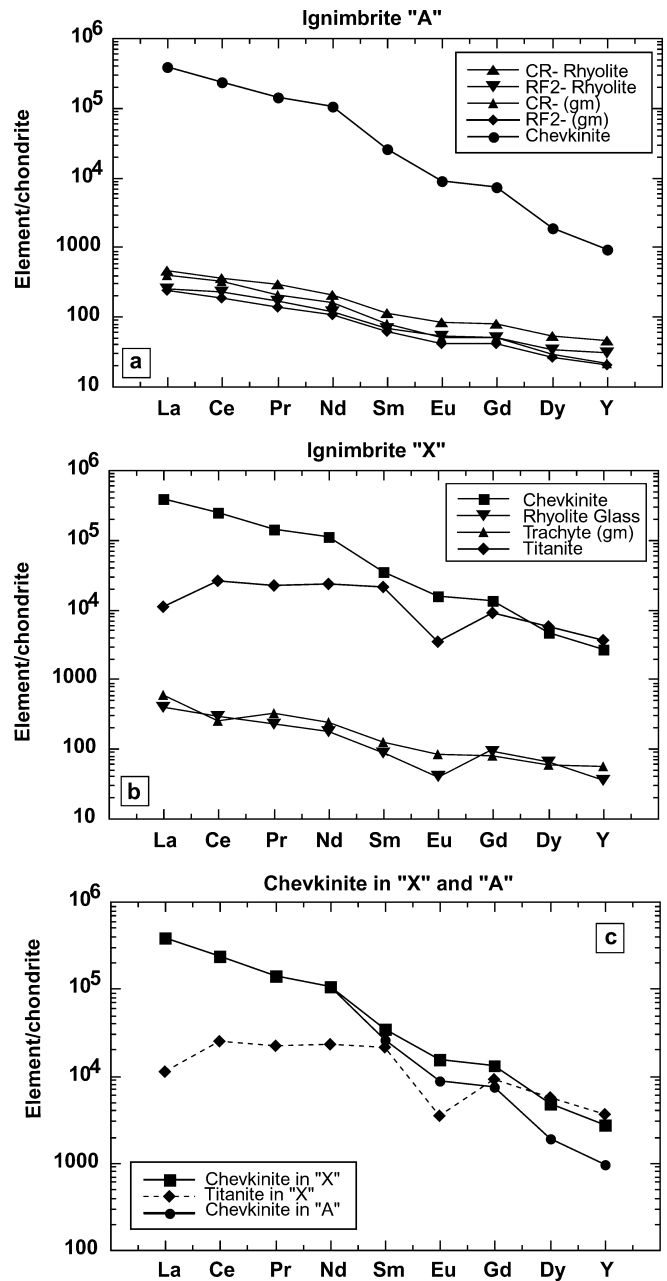


Fig. 4 Chondrite-normalised spider plots of **a** chevkinite, and rhyolite groundmass separates of ignimbrite "A", **b** chevkinite, titanite, rhyolite glass and trachyte groundmass, of ignimbrite "X" **c** chevkinites of ignimbrites "X" and "A" plus titanite from "X". Note the similarity in LREE concentrations of the two chevkinite examples, suggesting the phase to be insensitive to the presence of titanite as crystallising phase. In contrast to titanite, chevkinite lacks any major element anomalies such as the negative Eu anomaly, independently of the relative Eu concentrations in the melt

Nb in the mineral (compare Table 1). Zr/Nb in the whole rocks ranges from 7 to 10.5, and in groundmass separates from 8.5–12, from CR rhyolite to the most evolved RF2 rhyolite, respectively. There Nb partitioned preferentially into the mineral (relative to Zr), thus raising Zr/Nb ratios in the melt.

LREE, especially Ce, La and Nd concentrations in chevkinite from “A”, show—within the errors of the analytical method—virtually no difference to the concentrations of these elements in chevkinite from ignimbrite “X” (Fig. 4c), consistent with very similar La/Nd ratios in chevkinite from ignimbrite “A” (La/Nd=1.88) and “X” (La/Nd= 1.84). In contrast, HREE are somewhat depleted in chevkinite from ignimbrite “A”, a feature likely to be a function of lower HREE concentrations in the groundmass of ignimbrite “A” relative to ignimbrite “X” (Table 1).

Titanite in ignimbrite “X”

Titanite from the same syn-ignimbrite turbidite was analysed for comparison (Table 1). The Zr/Nb ratio of titanite is about 0.44, considerably lower than the Zr/Nb ratio of 1.55 in co-existing chevkinite, reflecting increased partitioning of Nb into titanite but similar partitioning of Zr into titanite and chevkinite. Titanite thus seems to preferentially accommodate Nb relative to Zr, suggesting that titanite crystallisation would have a strong impact on Zr/Nb ratios of residual liquids.

Enrichment of LREE in titanites is 1.5–2 orders of magnitude lower than that observed in chevkinite, but titanite contains slightly higher concentrations in HREE compared to chevkinite. The La/Nd ratio of titanite (La/Nd=0.24) is significantly lower than in chevkinite, implying that titanite fractionates MREE more strongly than LREE. Titanite also displays a more irregular pattern than chevkinite with a well-defined trough for Eu and $[La]_N < [Ce]_N$ (Fig. 4b, c), a pattern thought to be characteristic of titanite (Wörner et al. 1983; Green and Pearson 1986).

Partition coefficients

Apparent Kds for REE between chevkinite and melt and titanite and melt are given in Table 3. The high partition coefficients for LREE between chevkinite and melt reflect the enrichment of LREE of about three orders of magnitude relative to the glass, whereas titanite shows an LREE enrichment of only 1–1.5 orders of magnitude compared to the glass. The Kd_{REE} for chevkinite, moreover, shows a systematic decrease towards the

HREE and a comparatively smooth pattern on a chondrite-normalised spider plot (Figs. 4, 5). Titanite, in turn, shows an inhomogeneous Kd_{REE} distribution that does not systematically decrease with increasing atomic number (Fig. 5).

Discussion

Comparison of partition coefficients with other perrierite/chevkinite occurrences

Due to the lack of complete sets of partition coefficients for natural pairs of chevkinite and melt, comparison with other occurrences is difficult. Ewart (1982), for example, reported Kd_{Ce} values of 878–1,281 for a chevkinite/rhyolite pair from Australia, only slightly higher than our Kd_{Ce} value of 806 ± 30 . A perrierite in rhyodacite lava from Italy reported by van Bergen (1984) displays approximate Kd values of 880 for La and 1,057 for Ce, again similar to our data. Chevkinites from comenditic volcanic rocks of the East African Rift Valley studied by Macdonald et al. (2002) show a range of Kd_{Ce} of 1039–1472 and of Kd_{La} of 842–1293 in quartz trachyte to rhyolite, respectively, being somewhat higher than chevkinite/glass ratios from Gran Canaria. Macdonald et al. (2002) note, however, that the high values in their rhyolite-derived chevkinites are clearly at the REE-rich end of the compositional range of chevkinites and their lower values for trachyte-derived chevkinites are more representative for the intermediate range of chevkinite compositions.

Experimentally-derived Kd values of Green and Pearson (1988) confirm their prediction that their experimental Kd values may be about an order of magnitude too low. Green and Pearson derived a Kd_{La} of about 130 and a Kd_{Ce} of 85–90 at 900 °C, contrasting with the Kd values of 988 for La and 806 for Ce obtained in this study.

Unfortunately, little information on trace element partitioning between chevkinite and melt is available but chevkinites in comenditic lavas from the East African Rift Valley (Scaillet and Macdonald 2001; Macdonald et al. 2002) show Kd values of 26–56 for Nb and about 6 for Zr close to, but again somewhat higher than, our value of 15 ± 5 for Nb and ca. 3.5 for Zr. In contrast, van

Table 3 Element concentrations in chevkinite, titanite and associated glass

Element ppm (µg/g)	Sr	Y	Zr	Nb	La	Ce	Pr	Nd	Sm	Eu	Gd	Dy	Hf	Th
Chevkinite	504	5,595	4,120	2,650	117,600	190,268	16,911	63,971	6,678	1,127	3,402	1,507	85	755
Rhyolite glass	6	75.4	1,160	178	119	236	27	104	17	5	24	21	< 10	< 15
Titanite	51	7,466	3,623	8,230	3,418	20,400	2,646	14,000	4,095	250	2,316	1,718	–	–
$Kd=chevkinite$ glass	84	74	3.55	15	988	806	626	615	392	225	142	72	> 8.5	> 50
$Kd=titanite$ glass	± 22	± 25	± 0.4	± 5	± 30	± 30	± 30	± 40	± 50	± 30	± 25	± 20	–	–
$Kd=titanite$ glass	8.5	99	3.1	46	28	86	98	134	240	50	96	82	–	–
$Kd=titanite$ glass	± 1.5	± 30	± 0.5	± 10	± 10	± 20	± 30	± 35	± 50	± 20	± 25	± 25	–	–

± Values include 2σ analytical error and spread of analysis

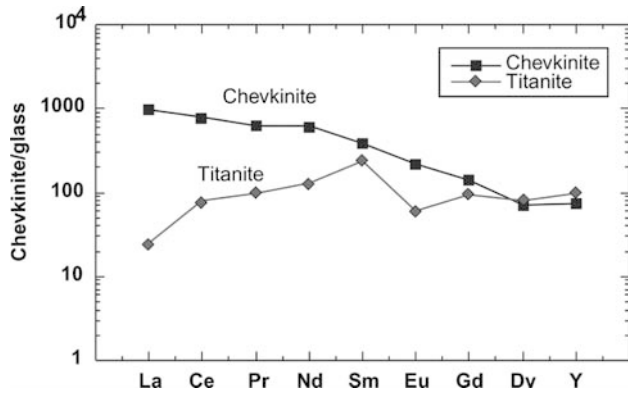


Fig. 5 REE partitioning between chevkinite and glass and titanite and glass in ignimbrite "X". Data are given in Table 3

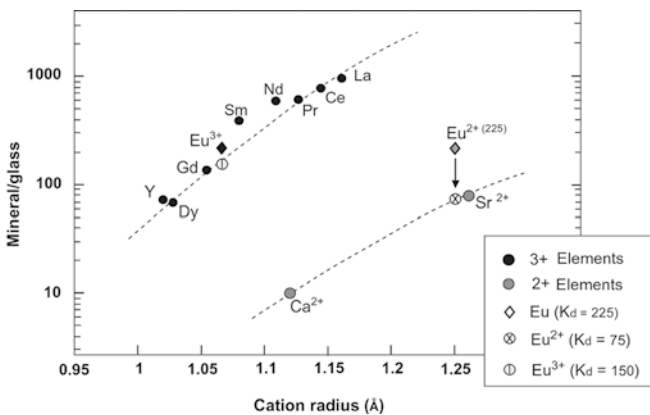


Fig. 6 Onuma diagram for divalent and trivalent elements that enter the chevkinite A-site (element radii are for eight-fold coordination after Shannon 1976). Elements that enter a specific site in the crystal lattice and have the same ionic charge exhibit generally smooth curves; curves for elements with different ionic charge that enter the same lattice site tend to be roughly parallel to each other. The *grey diamond* shows all Eu plotted as Eu^{2+} , the *black diamond* shows all Eu plotted as Eu^{3+} . Because the total $K_{d_{\text{Eu}}}$ comprises the partition coefficients of Eu^{2+} and Eu^{3+} , an estimate for $K_{d_{\text{Eu}^{2+}}}$ can be derived from the intersection of the divalent element curve with the ionic radius for Eu^{2+} (*crossed circle*). A $K_{d_{\text{Eu}^{2+}}}$ of ~ 75 is determined. This correlates well with a $K_{d_{\text{Sr}^{2+}}}$ of 84, reflecting the very similar geochemical behaviour of Sr and Eu^{2+} . The remaining $K_{d_{\text{Eu}^{3+}}}$ should be on the order of 150 (*dashed circle*)

Bergen (1984) reported a $K_{d_{\text{Zr}}}$ of 38 for perrierite/glass pair in calc-alkaline lavas from Italy, one order of magnitude higher than our result of $K_{d_{\text{Zr}}}=3.55$. This discrepancy is thought to be a function of ocean island magmas being generally REE-enriched relative to calc-alkaline magmas, reflected by van Bergen's glass containing 149 ppm Zr, whereas our glass contains 1,160 ppm Zr, but may also be strongly dependent on differing structural parameters that govern partitioning and/or different effects of melt polymerisation, temperature and volatile content in peralkaline versus calc-alkaline magmas in general.

Controls on chevkinite growth

P, T, X conditions

Perrierite/chevkinite has been experimentally grown from various REE-enriched melt compositions under a wide range of pressures and temperatures (Green and Pearson, 1988; Scaillet and Macdonald, 2001). In nature, however, the mineral occurs predominantly in alkaline to peralkaline syenites and granites and their eruptive equivalents i.e. trachytes and rhyolites. Recently, experimental phase relations for comendites from Kenya have been established by Scaillet and Macdonald (2001) for various P, T, X conditions. The derived pre-eruptive pressures, temperatures and H_2O contents for ignimbrites "A" and "X" are broadly within the range of chevkinite stability defined by Scaillet and Macdonald and plot within the chevkinite stability field of their sample "SMN 49" at 1.5 kb and $\log f_{\text{O}_2}$ of $\text{NNO} + 3.6$.

Chevkinite in the Mogan Group, however, formed only in some of the peralkaline rhyolitic to trachytic ignimbrites of the Middle to Upper Mogan Group, whereas e.g. zircon and \pm apatite are the REE-bearing phases in the sub-alkaline to mildly alkaline ignimbrites of the Lower Mogan Group. While chevkinite forms on REE saturation in H_2O -undersaturated to saturated magmas with high Ti and REE activity (Green and Pearson 1988), apatite may form in cases of additional high phosphorus activity (the more common situation). Alternatively, in the case of REE and H_2O saturation, coupled with a low Ti activity (e.g. following substantial removal of Fe-Ti oxides from the magma), allanite may be the stable REE mineral precipitating. Under similar conditions but with additional high Ca activity, apatite and monazite may form instead of allanite. This implies that the Mogan magmas that contain chevkinite had low P and Ca activities. Ca, a major constituent of plagioclase feldspar, was clearly low in the melt (Table 1) due to prolonged feldspar removal. P concentrations in the peralkaline Middle to Upper Mogan Group magmas (P_2O_5 up to 0.16 wt%) are generally lower than in the subalkaline magmas of the Lower Mogan Group (P_2O_5 up to 0.45 wt%).

Chevkinite and its chemical environment

The concentration of LREE in chevkinite is 1.5–2 orders of magnitude higher than in co-existing titanite, but HREE-concentrations are roughly the same. $K_{d_{\text{REE}}}$ for chevkinite show a systematic decrease towards the HREE and a relatively smooth pattern (Figs. 4, 5). Titanite, in turn, displays an inhomogeneous Kd distribution that does not systematically decrease with increasing atomic number, but rather shows a plateau for MREE on a broadly convex upward pattern (cf. Wörner et al. 1983; Green and Pearson 1986). Clearly chevkinite is more influential in the LREE budget of the melt than titanite. Moreover, the composition of chevkinite seems to be virtually independent of the

presence of titanite, since LREE concentrations of chevkinite in both ignimbrites, are virtually identical, although ignimbrite “X” contains titanite but ignimbrite “A” does not.

Chevkinite thus appears to act as a “REE sink” with strong attraction to all REE to the extent that these are readily accommodated in the chevkinite structure. The main substitution in the chevkinite A-site was previously identified as CaCe (e.g. Green and Pearson 1988; Macdonald et al. 2002), consistent with that in Gran Canaria chevkinites (see Fig. 6). According to the calculated Kd_{REE} , growing chevkinite extracts LREE into its A-site from a volume of magma about 10^3 times as large as its own volume and, moreover, it may extract these elements at a fairly constant rate over magmatic time scales, as evidenced by the absence of textural and compositional zoning in the chevkinite crystals.

Chevkinites from Gran Canaria also show no major dependence on the relative concentrations of Eu in the melt from which the mineral precipitated. Ignimbrite “X” rhyolite glass shows a negative Eu anomaly of $Eu/Eu^* \approx 0.7-0.75$, indicating feldspar removal with much of the Eu being available as Eu^{2+} . In ignimbrite “A”, groundmass separates of the rhyolites show far less pronounced negative Eu anomalies ($Eu/Eu^* \approx 0.85-0.9$). In both cases, chevkinite shows a systematic decrease of element concentrations with increasing atomic number, with similarly strong negative anomalies for Eu. This implies that the mineral is relatively insensitive to small-scale variations in availability and/or oxidation stage of Eu within the compositional range of Gran Canaria peralkaline melts.

On a plot of cation radius versus mineral/glass ratio (a so-called Onuma diagram, cf. Onuma et al. 1968) elements that enter a specific site in the crystal structure and have the same ionic charge generally exhibit smooth curves. Curves for elements with different ionic charge that enter the same lattice site tend to be roughly parallel to each other (Onuma et al. 1968; Blundy and Wood 1994; Wood and Blundy 1997). Onuma diagrams can therefore be used to estimate the size of a distribution coefficient when measurements have been made for an element that behaves very similar to the unknown. To evaluate the partitioning of Eu^{2+} relative to Eu^{3+} in Gran Canaria chevkinites we plotted the partition coefficients determined for elements that enter the A-site versus their ionic radii (Fig. 6). As the total Kd_{Eu} comprises the partition coefficients of Eu^{2+} and Eu^{3+} , an estimate for $Kd_{Eu^{2+}}$ can be derived from the intersection of the divalent element curve with the ionic radius for Eu^{2+} . A $Kd_{Eu^{2+}}$ of ~ 75 is determined. This correlates well with a $Kd_{Sr^{2+}}$ of 84, reflecting the very similar geochemical behaviour of Sr and divalent Eu. Since the bulk Kd for Eu in chevkinite is $Kd_{Eu} = 225$ and comprises $Kd_{Eu^{2+}}$ of 75, the remaining $Kd_{Eu^{3+}}$ should be on the order of 150, still correlating with the curve for trivalent elements in Fig. 6. Eu can thus be hosted in the

chevkinite A-site as both, divalent and trivalent Eu, with up to 33% of Eu being Eu^{2+} in Gran Canaria chevkinites.

The partitioning behaviour of REE into chevkinite probably allows chevkinite to compensate for smaller differences in melt chemistry and the presence or absence of other accessory phases. This behaviour of chevkinite is common, and chevkinite compositions tend to display surprising similarity over several magmatic pulses in the same magmatic system. For example, Harding et al. (1982) reported the occurrence of compositionally constant chevkinite in three granites from St Kilda/ Scotland, with each granite representing a different phase of intrusion and having a different chemical composition and a very different suite of accessory minerals, but with compositionally similar chevkinite in all three granites. Chevkinite can thus be considered as relatively insensitive to small scale fluctuations in REE abundance, Eu oxidation stage and the presence of other potentially REE-bearing phases throughout several pulses of a magmatic system, as long as melts are saturated in REE. Chevkinite is thus clearly the dominant LREE mineral in comenditic magmas on Gran Canaria. Titanite, in turn, seems to be more influential in the HREE evolution of the melt and behaves differently to chevkinite through the preferential accommodation of particular elements according to their relative availability, oxidation state or ionic radius.

Although chevkinite seems to be able to compensate for small fluctuations in P, T, and X within the same system, chevkinites from different localities, i.e. different volcanic systems, are in marked compositional contrast. For example, the composition of chevkinites from Gran Canaria differs markedly from Kenyan examples (Macdonald et al. 2002) which display a) a generally higher LREE content and b) more pronounced negative Eu anomalies (Kenyan chevkinites $Eu/Eu^* = 0.04$; Gran Canaria chevkinites $Eu/Eu^* \approx 0.65-0.75$). The causes for these major discrepancies are unknown but may include one or more of the following reasons: (1) concentrations of Eu are one order of magnitude lower in the Kenyan rhyolite glasses (ca. 0.15–0.5 ppm) relative to Gran Canaria rhyolite glass (3–5 ppm). (2) The Kenyan samples have most probably crystallised at lower temperatures ($\sim 785-660$ °C) than the Gran Canaria rhyolites ($\sim 800-750$ °C), which may have a drastic effect on the elasticity of the chevkinite A-site. (3) Oxygen activity was probably somewhat higher in the Kenyan rhyolites than in the Gran Canaria ones (cf. Scaillet and Macdonald 2001), suggesting that more Eu was present in the trivalent state in the Kenyan magmas.

This brief comparison between the Gran Canaria and the Kenyan samples shows that large variations in composition, temperature, and oxygen fugacity may have major effects on the partitioning of REE, contrasting the relative insensitivity of REE partitioning within individual volcanic systems and successive pulses of a volcanic suite.

Quantifying the effects of chevkinite crystallisation

Since perrierite and chevkinite are probably more widespread accessory minerals than hitherto assumed (e.g. Imaoka and Nakashima 1994), it is of increasing interest to accurately quantify their influence during magmatic evolution. Because perrierite and chevkinite act as REE-sinks, with little sensitivity to small changes in melt chemistry and the presence of other REE phases, we infer that the apparent Kd values reported here allow one to quantify roughly chevkinite crystallisation and melt evolution in Gran Canaria rhyolite magmas and, perhaps, similar occurrences elsewhere that fall within a similar P, T, X range. Our results suggest that the removal of only 0.05 wt% of chevkinite can fully account for both the reduction in Ce of ca. 100 ppm and that of La of ca. 60 ppm observed between the rhyolite end-members of ignimbrite "A" (cf. Fig. 2). Rigorous application of the Kd values determined to natural systems containing perrierite or chevkinite will therefore improve our understanding of the relevance of REE minerals in evolved magmas and shed light on their petrogenesis.

Acknowledgements During revision of the manuscript by the authors, Peter M. Sachs fell unexpectedly ill in December 2001 and passed away on July 9, 2002. Although all post-review changes were discussed with him and had his approval, he did not have the chance to comment on the final version of the manuscript. Peter was a great colleague and an enormous source of scientific inspiration. He will be missed dearly.

We thank F. Lechtenberg (SYXRF), O. Schneider (EMP) and D. Rau (XRF) for assistance and support during data acquisition and C. Harris is thanked for providing high quality oxygen isotope data. R. Macdonald is thanked for critical reading of an earlier version of the manuscript and for help with the structural formulae. Discussions with T.H. Hansteen, R. Seyfried, C. McKeon, W.E. Stephens and A. Freundt on various aspects of the manuscript are greatly appreciated. Frances Wall and John Wolff provided stimulating reviews and Ian Parsons is thanked for editorial handling. Financial support by the Deutsche Forschungsgemeinschaft (grant Schm 250/72-1,2) and a grant to VRT y the "Studienstiftung des deutschen Volkes" is gratefully acknowledged.

References

- Anderson JL, Smith DR (1995) The effect of temperature and oxygen fugacity on Al-in-hornblende barometry. *Am Mineral* 80:549–559
- Bennett JN, Turner DC, Ike EC, Bowden P (1984) The geology of some northern Nigerian anorogenic ring complexes. *Overseas Geol Miner Res* 61:1–65
- Blake S (1981) Eruptions from zoned magma chambers. *Geol Soc Lond* 138:281–287
- Blundy J, Wood B (1994) Prediction of crystal-melt partition coefficients from elastic moduli. *Nature* 372:452–454
- Bogaard Pvd, Schmincke H-U (1998) Chronostratigraphy of Gran Canaria. In: Weaver PPE, Schmincke HU, Firth JV, Duffield W (eds) *Proc ODP Sci Results* 157. Ocean Drilling Program, College Station, TX, pp 127–140
- Brooks CK, Henderson P, Rönso JG (1981) Rare-earth partitioning between allanite and glass in the obsidian of Sandy Braes, northern Ireland. *Mineral Mag* 44:157–160
- Cousens BL, Spera FJ, Tilton GR (1990) Isotopic patterns in silicic ignimbrites and lava flows of the Mogan and the lower Fataga Formations, Gran Canaria, Canary Islands: temporal changes in mantle source composition. *Earth Planet Sci Lett* 96:319–335
- Crisp JA, Spera FJ (1987) Pyroclastic flows and lavas of the Mogan and Fataga formations, Tejada volcano, Gran Canaria, Canary Islands: mineral chemistry, intensive parameters, and magma chamber evolution. *Contrib Mineral Petrol* 96:503–518
- Ewart A (1981) The Mineralogy and chemistry of the anorogenic Tertiary silicic volcanics of SE Queensland and NE New South Wales. *J Geophys Res* 86:10242–10256
- Ewart A (1982) Petrogenesis of the Tertiary anorogenic volcanic series of southern Queensland, Australia, in the light of trace element geochemistry and O, Sr and Pb Isotopes. *J Petrol* 23:344–382
- Freundt A, Schmincke H-U (1995) Petrogenesis of rhyolite-trachyte-basalt composite ignimbrite P1, Gran Canaria, Canary Islands. *J Geophys Res* 100: 455–474
- Green TH, Pearson NJ (1986) Rare-earth element partitioning between sphene and co-existing silicate liquid at high pressure and temperature. *Chem Geol* 55:105–119
- Green TH, Pearson NJ (1988) Experimental crystallisation of chevkinite/perrierite from REE-enriched silicate liquids at high pressure and temperature. *Mineral Mag* 52:113–120
- Haggerty SE, Mariano AN (1983) Strontian-lopaprite and strontio-chevkinite: two new minerals in reomorphic fenites from the Paraná Basin carbonatites, South America. *Contrib Mineral Petrol* 84:365–381
- Harding RR, Merriman RJ, Nancarrow PHA (1982) A note on the occurrence of chevkinite, allanite, and zirkelite on St Kilda, Scotland. *Mineral Mag* 46:445–448
- Hansteen TH, Sachs PM, Lechtenberg F (2000) Synchrotron-XRF microprobe analysis of silicate reference standards using fundamental parameter quantification. *Eur J Mineral* 12:25–31
- Harris C, Smith HS, le Roex A (2000) Oxygen isotope composition of phenocrysts from Tristan da Cunha and Gough Island lavas: variation with fractional crystallization and evidence for assimilation. *Contrib Mineral Petrol* 138:164–175
- Helz RT (1979) Alkali exchange between hornblende and melt: a temperature sensitive reaction. *Am Mineral* 64:953–965
- Hoefs J (1996) *Stable isotope geochemistry*. Springer, Berlin Heidelberg New York, pp 1–201
- Hoernle K, Schmincke H-U (1993) The role of partial melting in the 15 Ma geochemical evolution of Gran Canaria: a blob model for the Canary hotspot. *J Petrol* 34:599–626
- Imaoka T, Nakashima K (1994) Chevkinite in syenites from Cape Ashizuri, Shikoku Island, Japan. *Neues Jahrb Miner Monatsh* 8:358–366
- Ito J (1967) A study of chevkinite and perrierite. *Am Mineral* 52:1094–1104
- Izett GA, Wilcox RE (1966) Perrierite, chevkinite and allanite in Upper Cenozoic ash beds in the western United States. *Am Mineral* 33:1558–1567
- Jaffe HW, Evans HT, Chapman RW (1956) Occurrence and age of chevkinite from the Devil's Slide fayalite quartz syenite near Stark, New Hampshire. *Am Mineral* 41:474–487
- Janssens K, Vincze L, van Espen P, Adams F (1993) Monte Carlo simulation of conventional and synchrotron energy dispersive X-ray spectrometers. *X-Ray Spectrom* 22:234–243
- Johnson MC, Rutherford MJ (1989) Experimental calibration of the aluminum-in-hornblende geobarometer with application to the Long Valley caldera (California) volcanic rocks. *Geology* 17:837–841
- Lechtenberg F, Garbe-Schönberg D, Bauch J, Dingwell DB, Freitag J, Haller M, Hansteen TH, Knöchel A, Radtke M, Romano C, Sachs PM, Schmincke H-U, Ullrich HJ (1996) The X-ray fluorescence measurement place at beamline L of HASYLAB. *Trace Microanalyst Techn* 14:561–587
- Macdonald R (1974) Nomenclature and petrochemistry of the peralkaline oversaturated extrusive rocks. *Bull Volcanol* 38:498–516
- Macdonald R, Marshall AS, Dawson JB, Hinton RW, Hill PG (2002) Chevkinites from silicic volcanic rocks of the East African Rift. *Mineral Mag* 66:287–299

- Mahood GA (1981) Chemical evolution of a Pleistocene rhyolite center: Sierra La Primavera, Jalisco, Mexico. *Contrib Mineral Petrol* 77:129–149
- Mitchell RS (1966) Virginia metamict minerals: perrierite and chevkinite. *Am Mineral* 51:1394–1405
- Onuma N, Higuchi H, Wakita H, Nagasawa H (1968) Trace element partitioning between two pyroxenes and the host lava. *Earth Planet Sci Lett* 5:47–51
- Platt RG, Wall F, Williams CT, Woolley AR (1987) Zirconolite, chevkinite and other rare earth minerals from nepheline syenites and peralkaline granites and syenites of the Chilwa Alkaline Province, Malawi. *Mineral Mag* 51:253–263
- Pouchou JL, Pichoir F (1984) A new model for quantitative X-ray microanalysis, Part I. Application to the analysis of homogeneous samples. *Rech Aerospac* 3:13–38
- Robinson DM, Miller CF (1999) Record of magma chamber processes preserved in accessory mineral assemblages, Aztec Wash pluton, Nevada. *Am Mineral* 84:1346–1353
- Sachs PM, Hansteen TH (2000) Pleistocene underplating and metasomatism of the lower continental crust: a xenolith study. *J Petrol* 41:331–356
- Segelstad TV, Larson AO (1978) Chevkinite and perrierite from the Oslo region, Norway. *Am Mineral* 63:499–505
- Scaillot B, Macdonald R (2001) Phase relations of peralkaline silicic magmas and petrogenetic implications. *J Petrol* 42:825–845
- Shannon RD (1976) Revised effective ionic radii and systematic studies of interatomic distances in halides and chalcogenides. *Acta Crystallogr A* 32:751–767
- Schirnack C, Bogaard P v. d., Schmincke H-U (1999) Cone sheet formation and intrusive growth of an oceanic island—The Miocene Tejada complex on Gran Canaria (Canary Islands). *Geology* 27:207–210
- Schmincke H-U (1997) Geological field guide of Gran Canaria: Parts I and II. Pluto Press, Ascheberg, pp 1–64
- Schmincke H-U (1976) The geology of the Canary Islands. In: Kunkel G. (ed) *Biogeography and ecology in the Canary Islands*. W Junk, BV Publ, The Hague, pp 67–184
- Schmincke H-U (1969) Petrologie der phonolithischen bis rhyolithischen Vulkanite auf Gran Canaria, Kanarische Inseln. Habilitationsschrift, Universität Heidelberg, pp 1–151
- Silver LA, Ihinger PD, Stolper E (1990) The influence of bulk composition on the speciation of water in silicate glasses. *Contrib Mineral Petrol* 104:142–162
- Sumita M, Schmincke H-U (1998) Tephra event stratigraphy and emplacement of volcanoclastic sediments. Mogan and Fataga stratigraphic intervals, Part I: mineral and chemical stratigraphy of volcanoclastic units and correlation to the subaerial record. In: Weaver PPE, Schmincke H-U, Firth JV and Duffield W (eds) *Proc ODP Sci Results* 157. Ocean Drilling Program. College Station, TX, pp 219–266
- Thomas R (1990) Abschätzung der Bildungstemperatur magmatischer Schmelzen. *Z Geol Wissensch* 18:5–14
- Troll VR, Sachs PM, Lechtenberg F, Schmincke H-U, Sumita M (1999) The role of the accessory REE mineral chevkinite/perrierite on the rare earth and trace element budget of evolved peralkaline magmas: an example from Gran Canaria. *HASYLAB Annual Report 1999: Hamburger Synchrotronstrahlungslab HASYLAB Deutsches Elektronen-synchrotron DESY*, pp 993–994
- Troll VR (2001) Evolution of large peralkaline silicic magma chambers and associated caldera systems; a case study from Gran Canaria, Canary Islands. PhD Thesis, Christian-Albrechts Universität Kiel, pp 1–143
- Troll VR, Schmincke H-U (2002) Magma mixing and crustal recycling recorded in ternary feldspar from compositionally zoned peralkaline ignimbrite “A”, Gran Canaria, Canary Islands. *J Petrol* 43:243–270
- van Bergen MJ (1984) Perrierite in siliceous lavas from Mt Amiata, central Italy. *Mineral Mag* 48:553–556
- Vincze L, Janssens K, Adams F (1993) A general Monte Carlo simulation of energy dispersive X-ray fluorescence spectrometers—Part I. *Spectrochim Acta* 48:553–573
- Wolff JA, Storey M (1984) Zoning in highly alkaline magma bodies. *Geol Mag* 121:563–575
- Wones DR (1981) Biotites and amphiboles in igneous rocks: Dehydration redox reactions. In: Veblen DR, Ribbe PH (eds) *Amphiboles: Petrology and experimental phase relations*. *Rev Mineral* 9B: 357–371
- Wones DR (1989) Significance of the assemblage titanite + magnetite + quartz in granitic rocks. *Am Mineral* 74:744–749
- Wood B, Blundy J (1997) A predictive model for rare earth element partitioning between clinopyroxene and anhydrous silicate melt. *Contrib Mineral Petrol* 129:166–181
- Wörner G, Beusen J-M, Duchateau N, Gijbels R, Schmincke H-U (1983) Trace element abundances and mineral/melt distribution coefficients in phonolites from the Laacher See Volcano (Germany). *Contrib Mineral Petrol* 84:152–173